ELSEVIER

Journal of Alloys and Compounds 216 (1994) 159–175

Journal of ALLOYS AND COMPOUNDS

Review

Hydriding kinetics of powders

Moshe H. Mintz[a,b], Yehuda Zeiri[a]

[a]*Nuclear Research Center, Negev, PO Box 9001, Beer-Sheva, Israel*

[b]*The Ben-Gurion University of the Negev, Department of Nuclear Engineering, PO Box 653, Beer-Sheva, Israel*

Received 18 March 1994; in final form 9 May 1994

Abstract

Kinetic measurements of gas–solid reactions performed on powders, are usually interpreted according to single-particle analysis (SPA) models. The use of SPA functions is not a priori justified, since deviations from that functional dependence may occur in the powder, owing to three factors: (i) particle size distributions, (ii) particle shape variations and (iii) time distributions for the beginning of the reaction on each one of the particles composing the powder. The effects of these factors are quantitatively analysed and their interference in the SPA procedure is estimated. It is concluded that under certain circumstances the SPA can yield the correct reaction mechanism and even enables a reasonable estimate of the corresponding intrinsic kinetic parameters. This analysis is relevant generally to gas–solid kinetics, with particular emphasis on hydriding reactions.

Keywords: Hydriding kinetics; Powders; Single-particle analysis

1. Introduction

Numerous kinetic studies on gas–solid reactions in general, and more specifically on hydriding–dehydriding reactions of powdered metallic samples, have been presented in the literature during the last two decades. Most of these studies were related to intermetallic hydrides systems (for a recent review see [1]), whereas a few dealt with binary hydrogen–metal reactions (see for example [2]). In any case, when different investigations performed on some given systems are compared, confusing and diverse kinetic results are obtained, casting serious doubts on the mechanistic interpretations of these studies. For example, comparing different results on the well-studied $LaNi_5$–hydrogen system, a variety of reaction rates, proposed rate laws and related mechanisms have been reported [3–11]. Some of these discrepancies were attributed to heat transfer effects resulting in non-isothermal conditions [10]. Indeed, such effects may lead to erronous kinetic rate laws, as demonstrated by Dantzer and Orgaz [12, 13]. However, even when controlled heat transfer conditions were applied [4,5,7,8], inconsistent results still occurred.

It has been pointed out [14] that in order to evaluate intrinsic kinetic parameters (i.e. the parameters which are not dependent either on geometrical factors or on reaction time, thus specifying the intrinsic kinetics of the given reacting system, under the given pressure–temperature conditions) in a reliable manner, the kinetic measurements should be performed on massive samples, with well defined geometrical shapes (e.g. plates, cubes, cylinders or spheres). For such samples, when reacted under certain experimental conditions which lead to the progression of the reaction by a "contracting envelope" (or "shrinking core") morphology, simple exact analytical expressions relate the measured overall kinetics (i.e. the total reacted fraction α vs. time curves) to the intrinsic kinetic parameters of the system. The different choices of these intrinsic parameters are summarized in [14] for different possible types of kinetics. For example, for a constant (time-independent) velocity U of the hydride–metal interface, this parameter is appropriate for characterizing the reacting system. For a time-dependent velocity, other intrinsic kinetic parameters may be chosen. The pressure–temperature dependence of these kinetic parameters may then point to the microscopic mechanism controlling the reaction rate [14–19].

For simple geometrical shapes of the reacting samples, the relation between the overall reacted fraction α and the reaction displacement $X(t)$ (at a given time t) is given by [14,20–22]

SSDI 0925-8388(94)01269-N

$$\alpha(t) = \sum_{i=1}^{3} a_i X^i(t) \quad (1)$$

where a_i are constants related to the shape and initial dimensions of the reacting samples, and $X(t)$ is given by

$$X(t) = X_0 + \int_{t_0}^{t} U(t)\, dt \quad (2)$$

with $U(t)$ the velocity of the hydride–metal interface (which may be either time dependent, e.g. for some diffusion-controlled cases, or constant [14], t_0 being the time required to form first a continuous hydride layer on the sample surface, and X_0 the initial thickness of that layer when formed at t_0 (Fig. 1). Hence, for the time interval between t_0 and t, Eq. (1) allows for the exact evaluation of $X(t)$ vs. t, from the measured values of the overall reacted fraction $\alpha(t)$. A plot of $X(t)$ vs. t yields then the hydride front velocity $U(t)$ (given by the slope of that curve), which as mentioned above is the intrinsic kinetic parameter for the case of a constant (time-independent) velocity.

It should be pointed out that for $t < t_0$, i.e. before a continuous product layer has been formed on the sample, no simple expression (such as Eq. (1)) can be utilized to relate the overall (measured) reacted fraction $\alpha(t)$ and any intrinsic kinetic parameter. Hence the quantitative interpretation of the kinetic data in that initial range is not possible in most cases, and only qualitative trends may be estimated. The reliable application of Eq. (1) for the evaluation of the hydride–metal interface velocity U therefore requires that X_0 be small compared with the initial dimensions of the reacting sample. Such requirement may not always be fulfilled, especially for small-size samples (e.g. thin foils or fine-particle powders). This point will further be discussed later.

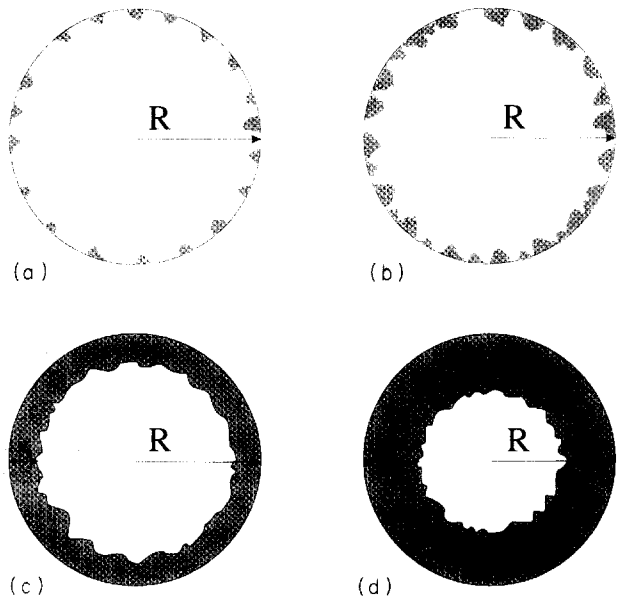

Fig. 1. Schematic illustration of the development of a product layer on a spherical reacting particle with an initial radius R: (a) nucleation on the surface; (b) nuclei growth and partial overlap; (c) initial formation of a continuous product layer (with an average thickness X_0) at time t_0; (d) further thickening of the layer at time t.

In certain cases, when the size of the sample can be specified by a single dimensional parameter R, Eq. (1) can be replaced by a relation of the form [14,20–22]

$$F_{r,g}(\alpha) = \frac{k}{R^n} t \quad (t > t_0) \quad (3)$$

where $F_{r,g}(\alpha)$ is a specified function of the reacted fraction. The subscript r indicates that the form of that function depends on the type of reaction kinetics (e.g. kinetics with the constant U, or diffusion-controlled kinetics with the time-dependent $U(t)$ etc.) and the subscript g that it depends on the geometrical shape of the sample (e.g. a cube, sphere or wire). k is a constant (e.g., for a time-independent interface velocity, k is proportional to U), and n is an integer (1 or 2) related to the type of kinetics.

As for Eq. (1), Eq. (3) is applicable only after the completion of a continuous product layer with an initial thickness of X_0 (Fig. 1), i.e. for $t > t_0$. The corresponding applicable α range thus depends on the relative magnitudes of X_0 and R. For $X_0/R \ll 1$, Eq. (3) is fulfilled over a wide range of α values whereas, for $X_0/R \approx 1$, Eq. (3) cannot be applied.

Let us consider now the utilization of the two above relations (i.e. Eqs. (1) and (3) respectively) for the analysis of kinetic data. When single well-defined geometrical samples are used [14–19], the application of Eq. (1) is preferred, since the different constants (i.e. the a_i values) are known (from the given dimensions of the samples), and an $X(t)$ vs. t curve may simply be calculated from the $\alpha(t)$ data, without any necessary assumptions on the controlling mechanism. This $X(t)$ curve then directly points to the type of controlling kinetics (i.e. whether U is constant or time dependent). Evidently, when the type of kinetics is established, the validity of the appropriate relation of the form given by Eq. (3) can be checked. On the other hand, when powdered samples are used, Eq. (1) cannot be utilized any more, since neither the shape nor the size of the sample is defined, and no unique a_i set can be specified. Yet, in an attempt to interpret gas–powder reaction kinetics, functions of the form given by Eq. (3) are usually fitted to the experimental data, with the approach that this functional dependence (originally derived for a single well-defined reacting particle) is still valid for an ensemble of particles with size distributions as well as shape variations. In other words, such dispersed powders can be well represented by fictitious ensembles of uniformly sized particles with a certain fixed shape

(e.g. spheres). Obviously, such an assumption cannot a priori be justified, and the above approach has been criticized in the literature [23–25], pointing to possible erroneous or perhaps indeterminate results concerning reaction mechanisms and activation energies, deduced by the simplified above procedure.

In this work, the deviations introduced into the single-particle analysis (SPA) by the different factors characterizing real powders are estimated. These factors include (1) particle size distributions, (2) particle shape variations and (3) time distributions for the commencement of the reaction on different particles, composing the powder. Two SPA models are applied, a constant-velocity contracting-envelope model, and a diffusion-controlled time-dependent-velocity model. The above calculations indicate under which powder characteristics and reaction conditions a reliable distinction between the two models may still be possible, utilizing a simple SPA procedure. It has been shown [25] that, under certain conditions, apparent activation barriers can be evaluated, even without knowledge of either the controlling mechanism or the powder particle size distribution. In these cases it is shown here that an evaluation of the proper mechanism is also possible by the SPA procedure, without any consideration of size or shape distributions. However, this simplified SPA procedure is limited to reactions where the time distributions for the initiation of reaction on the different powder particles are much smaller than the corresponding reaction half-times $t_{1/2}$, and where a contracting-envelope morphology is attained for very small α values (i.e. when X_0 is much smaller than the particles size).

In contrast with the above contracting-envelope morphology, where all the product forms a defined film (developing from the outer surface into the bulk), the extreme opposite case is that of random nucleation and growth in the bulk, where the product is dispersed evenly within the reacting particle. In this case, the kinetic equations should evidently be independent of the sample's geometrical shape or size. The evaluation of such analytical kinetic functions is not as simple as for the contracting-envelope cases, and only approximate relations can be obtained [26–28]. The most utilized functions of this type are the Avrami–Erofeyev functions, given in Section 2. In order to complete the kinetic analysis of powders, this case is also included.

It should be emphasized that self-heating problems, encountered in many kinetic experiments performed on powders, are not considered here and isothermal conditions are assumed. It is evident that the interference of self-heating effects will modify the measured kinetics in such a complex way that no meaningful analysis can then be made.

The following analysis is pertinent in general to a variety of gas–solid reactions; however, specified examples on hydride systems are demonstrated.

2. Calculation procedures

2.1. Single-particle analysis

Before discussing powder analysis, some reminder of SPA may be helpful. As mentioned in Section 1 for a contracting-envelope progression, functions of the form given either by Eq. (1) or alternatively by Eq. (3) relate the reacted fraction α to the reaction time t. A summary of these functions is given in the literature [14,20–22]. Since the common approach to powder analysis assumes the powders to consist of spherical particles, we shall specify now Eqs. (1) and (3) for this geometry only. The kinetic classes are then analysed for the contracting-envelope cases, and a third class (the Avrami–Erofeyev type) for the random nucleation and growth in the bulk.

For the contracting-envelope progression, one possible case is of a constant interface velocity U (henceforth denoted by the subscript CV) where the kinetic functions are given either by

$$\alpha_{CV}(t)=1-\left(1-\frac{U}{R}t\right)^3=\frac{3U}{R}t-\frac{3U^2}{R^2}t^2+\frac{U^3}{R^3}t^3 \qquad (4)$$

or, by rearranging Eq. (4)

$$F_{CV}(\alpha)=1-[1-\alpha(t)]^{1/3}=\frac{U}{R}t \quad \left(0\leqslant t\leqslant\frac{R}{U}\right) \qquad (5)$$

For small α values, i.e. $\alpha\ll 1$,

$$F_{CV}(\alpha\ll 1)\approx\frac{1}{3}\alpha(t)=\frac{U}{R}t \qquad (5')$$

which represents the linear term in Eq. (4).

The other possible type of kinetics for the contracting-envelope case is that of a decelerating velocity, controlled by the diffusion of gas atoms through the thickening product layer (henceforth denoted by the subscript D). The kinetic function is then given by the Carter–Valensi expression [29,30]

$$F_D(\alpha)=\frac{\epsilon-[1+(\epsilon-1)\alpha(t)]^{2/3}-(\epsilon-1)[1-\alpha(t)]^{2/3}}{\epsilon-1}$$

$$=2\frac{k_D}{R^2}t$$

$$\left(0\leqslant t\leqslant\frac{\epsilon^{2/3}}{2(\epsilon^{2/3}+\epsilon^{1/3}+1)}\frac{R^2}{k_D}\right) \qquad (6)$$

where ϵ is the product-to-reactant-volume ratio and k_D a diffusion-related constant, chosen as the intrinsic kinetic parameter for this case. For hydrogen–metal

reactions, k_D is given by [14]

$$k_D(P, T) = \frac{1}{\epsilon} \frac{Z_0(P, T)}{y(T)} D(T) \quad (7)$$

where P is the hydrogen working pressure, T (K) the reaction (absolute) temperature, $y(T)$ the hydride composition limit (at T), $Z_0(P, T)$ the equilibrium excess hydrogen composition (i.e. that hydrogen which dissolves in the hydride at the given P–T) and $D(T)$ the diffusivity of hydrogen in the hydride.

It is worthwhile to mention that in some studies [21] the so-called Jander equation is utilized to represent the above decelerating (diffusion-controlled) kinetics. This Jander function, however, is based on the incorrect assumption that the radius of the spherical shrinking core obeys a square-root time dependence, similar to the diffusion-controlled planar case. Hence,

$$F_D(\alpha) = [F_{CV}(\alpha)]^2 = kt \quad (8)$$

with $F_{CV}(\alpha)$ – given by Eq. (5) and k – a diffusion-related constant. Evidently, the utilization of planar kinetics to the spherical geometry is not justified, and the proper diffusion equation should be solved, leading to the above Carter–Valensi relation (Eq. (6)).

It is possible, however, to simplify Eq. (6), for cases where $\epsilon \to 1$ (i.e. where the volume change associated with the product formation is not large). In these cases, $(\epsilon - 1)\alpha(t) \ll 1$, a series expansion of $[1 + (\epsilon - 1)\alpha(t)]^{2/3}$ reduces Eq. (6) to

$$F_D(\alpha) \approx 1 - \frac{2}{3}\alpha(t) - [1 - \alpha(t)]^{2/3} = \frac{2k_D}{R^2} t \quad \left(0 \leqslant t \leqslant \frac{R^2}{6k_D}\right) \quad (9)$$

The latter simplified form will be utilized henceforth for the analysis of the decelerating-velocity diffusion-controlled kinetics. It is interesting to point out that, for $\alpha \ll 1$, expanding $F_D(\alpha)$ in Eq. (9) to a Taylor series and taking terms up to quadratic yield

$$F_D(\alpha \ll 1) \approx \frac{1}{9}\alpha^2(t) = \frac{2k_D}{R^2} t \quad (9')$$

which displays the square-root-of-time α dependence typical of planar geometry [14] but with a different slope, as discussed further in Section 2.2.2.

The alternative form of Eq. (9), corresponding to the $\alpha_D(t)$ vs. t kinetic curves, can be derived by substituting into Eq. (9):

$$\xi(t) = [1 - \alpha(t)]^{1/3} \quad (10)$$

Eq. (9) then assumes the form

$$\xi^3 - 1.5\xi^2 + \left(0.5 - \frac{3k_D t}{R^2}\right) = 0 \quad (11)$$

Solution of the cubic Eq. (11) yielding the physically meaningful root $\xi_0(t)$ $(0 \leqslant \xi_0 \leqslant 1)$ is then calculated (for any given t) and substituted into Eq. (10), leading to

$$\alpha_D(t) = 1 - \xi_0^3(t) \quad (12a)$$

with

$$\xi_0(t) = 0.5 + \cos\left[\theta(t) + \frac{4}{3}\pi\right] \quad (12b)$$

$$\theta(t) = \frac{1}{3}\cos^{-1}\left(\frac{12k_D}{R^2} t - 1\right) \quad \left(0 \leqslant t \leqslant \frac{R^2}{6k_D}\right) \quad (12c)$$

Finally, for random bulk nucleation and growth (henceforth denoted by the subscript NG), the most utilized approximation is the Avrami–Erofeyev type of function given by [26–28]

$$\alpha_{NG}(t) = 1 - \exp(-k_{NG} t^n) \quad (n \geqslant 2) \quad (13)$$

$$k_{NG} = K_g N_0 U^n$$

or alternatively by

$$F_{NG}(\alpha) = \{-\ln[1 - \alpha(t)]\}^{1/n} = k_{NG}{}^{1/n} t \quad (14)$$

where K_g is a constant which is dependent on the geometrical shape of the growing nuclei (e.g. $\frac{4}{3}\pi$ for spheres, and 8 for cubes) but is independent of the reacting sample geometry, N_0 is the number of available nucleation sites per unit volume of the sample, n is an integer number (related to the dimensionality of the growth process) and U is the growth velocity of a growing nuclei.

In the following discussion, it is convenient to utilize a reduced time scale τ defined by

$$\tau = \frac{t}{t_{1/2}} \quad (15)$$

with $t_{1/2}$ the time required to reach $\alpha = \frac{1}{2}$. It is evident that any kinetic function which may be expressed in the form of

$$F_r(\alpha) = k' t \quad (16)$$

(with r denoting the specific functional form related to the corresponding type of kinetics, e.g. Eq. (5), or Eqs. (6) and (9) or Eq. (14), and k' some rate constant) can also be expressed as

$$F_r(\alpha) = F_r(0.5)\tau \quad (17)$$

with $F_r(0.5)$ a given number obtained by substituting $\alpha = 0.5$ into $F_r(\alpha)$. Hence, for each of the above-mentioned types of kinetics, a plot of $F_r(\alpha)$ vs. τ should give a straight line with a fixed "universal" slope related only to the corresponding type of kinetics (i.e. independent of the reaction intrinsic kinetic parameters and the sample's size). These "universal" slopes are summarized in Table 1. Also are summarized the appropriate reduced time ranges corresponding to

Table 1
Summary of the characteristics of the different functional forms utilized for gas–solid kinetics (spherical geometry)

Type of kinetics (r)	Functional time dependence ($F_r(\alpha)$ vs. t)	Slope of reduced time representation (Eq. (17))	Reduced time range[a]
Contracting envelope with a constant interface velocity (r≡CV)	Eq. (5)	0.21	$0\leqslant\tau_{CV}\leqslant 4.8$ $0\leqslant\tau_{CV}^{*}\leqslant 3.8$
Contracting envelope with a decelerating velocity, controlled by diffusion through an adherent thickening product layer (r≡D)	Eq. (6) (Carter–Valensi)	$\frac{0.37\epsilon}{\epsilon-1}-\frac{0.63(\epsilon+1)^{2/3}}{\epsilon-1}+\frac{0.63}{\epsilon-1}$	
	or simplified form (for $\epsilon\rightarrow 1$) Eq. (9)	0.037	$0\leqslant\tau_{D}\leqslant 9$ $0\leqslant\tau_{D}^{*}\leqslant 8$
Random bulk nucleation and growth (r≡NG)	Eq. (14) (Avrami–Erofeyev)		$0\leqslant\tau_{NG}\leqslant\infty$ $0\leqslant\tau_{NG}^{*}\leqslant 2.6$
	$n=2$	0.833	$0\leqslant\tau_{NG}^{*}\leqslant 1.9$
	$n=3$	0.885	$0\leqslant\tau_{NG}^{*}\leqslant 1.6$
	$n=4$	0.921	

[a] τ_r denotes the range corresponding to $0\leqslant\alpha\leqslant 1$ whereas τ_r^{*} denotes the range corresponding to $0\leqslant\alpha\leqslant 0.99$.

$0\leqslant\alpha\leqslant 1$, which are given by

$$0\leqslant\tau_r\leqslant\frac{F_r(1)}{F_r(0.5)} \tag{18}$$

For the bulk nucleation-and-growth kinetics, even though $\alpha\rightarrow 1$ corresponds to $\tau_{NG}\rightarrow\infty$, practically it is sufficient to carry out the calculations within the range where $0\leqslant\alpha\leqslant 0.99$, which corresponds to the reduced time range below about 2–2.6 (depending on the value of n). In fact, the latter $0\leqslant\alpha\leqslant 0.99$ reduced time ranges (denoted as τ_r^{*} in Table 1) related to the nucleation-and-growth kinetics are shorter than those of the contracting-envelope kinetics. These time ranges $\{\tau_r^{*}\}$ follow the order

$$\{\tau_{NG}^{*}\}<\{\tau_{CV}^{*}\}<\{\tau_{D}^{*}\} \tag{19}$$

It is worthwhile to point to a qualitative feature which enables a simple distinction between the two groups of kinetics, namely the contracting-envelope kinetic functions and the bulk nucleation growth functions. Whereas the types of contracting-envelope kinetics (i.e. Eqs. (4) and (12)) display α vs. t curves with gradually decreasing slopes, the bulk nucleation and growth functions (Eq. (13)) display an S-shape with an inflection point (i.e. a maximum slope), which corresponds to the reduced time (τ_m):

$$\tau_m(n)=\left(\frac{n-1}{0.693n}\right)^{1/n}\quad(n\geqslant 2) \tag{20}$$

For $n=2$, 3 and 4, the corresponding τ_m are 0.85, 0.99 and 1.02 respectively. Hence, regardless of the value of the nucleation-and-growth rate constant k_{NG}, the inflection points in the $\alpha_{NG}(t)$ functions are located at about $t_{1/2}$ (i.e. displayed at reaction times close to that required to reach $\alpha\approx\frac{1}{2}$). Thus a qualitative quick distinction between the above two groups of kinetics is possible by just observing the shape of the experimental α vs. t curves. It may be argued that the occurrence of initial induction periods as well as initial surface nucleation-and-growth processes (preceding the formation of a continuous product film) may practically result in some turning points also in the α vs. t curves related to the contracting-envelope kinetics (i.e. as mentioned in section 1 the fit of Eqs. (5), (6) or (9) may start not at $t=0$ but after a certain t_0). These turning points, however, differ from the inherent turning points in the nucleation-and-growth functions by (i) occurring at low α (and t) values, far below the $\alpha\approx 0.5$ ($t\approx t_{1/2}$) values typical of the nucleation and growth processes, (ii) being much sharper, resembling a break point rather than inflection and (iii) depending on the size (and shape) of the reacting samples. In fact, the latter difference is valid not only for the turning-point

values but also for the whole $\alpha(t)$ vs. t curves, which for the contracting-envelope cases depend on the size and shape of the reacting samples (reacted under given experimental conditions), whereas for the nucleation-and-growth cases do not depend on size and shape factors.

It will be pointed out later on (Section 3) that there may occur some special cases where the $\alpha(t)$ vs. t curves obtained for well-defined (single-particle) samples do not depend on the size and shape of the reacting samples and yet obey contracting-envelope type of kinetics (and not nucleation-and-growth kinetics).

2.2. Powder analysis

In the following calculations the effects of three parameters which assume a single defined value in the SPA cases, but some spread values (i.e. some distribution functions) in powders, are evaluated. These parameters are (i) size, (ii) geometrical shape and (iii) initial reaction time. Evidently, each one of these parameters may vary for the different particles composing the powder. An analysis is thus made in order to estimate the influence of such variations on the SPA functions discussed before. The main questions addressed to these cases are the following.

(1) Can the overall kinetics (i.e. the $\alpha(t)$ vs. t curves) still be represented by the corresponding SPA-like functions (e.g. Eqs. (5) and (9))?

(2) If these SPA functions are still applicable, what are the corresponding slopes of these lines?

In the following analysis we shall utilize only the contacting-envelope cases (Eqs. (5) and (9)), since the nucleation-and-growth kinetics are inherently independent of the size and shape parameters.

2.2.1. Effects of size distributions

Assume a powder composed of spherical particles having a given size distribution $D(R)$. Assume further that all particles start to react at the same time, $t=0$. Each reacting particle i satisfies a given contracting-envelope type of kinetics r, e.g. as given by Eq. (4) (r ≡ CV) or by Eq. (12) (r ≡ D). Thus, for the ith powder's particle,

$$\alpha_i(t)=\alpha_r(R_i, t) \tag{21}$$

with $\alpha_r(R_i, t)$ given by the above contracting-envelope equations. The reacted volume of the ith particle is given by

$$v_i(t)=\frac{4}{3}\pi R_i^3\alpha_i(t)=\frac{4}{3}\pi R_i^3\alpha_r(R_i, t) \tag{22}$$

and the number of particles with the size ranging between R_i and $R_i+\mathrm{d}R$ are

$$\mathrm{d}N_i=D(R_i)\,\mathrm{d}R \tag{23}$$

Hence, the total reacted volume at time t, integrated over all powder particles, is given by

$$V_r(t)=\frac{4}{3}\pi\int_{R_{min}}^{\infty}D(R)R^3\alpha_r(R, t)\,\mathrm{d}R \tag{24}$$

with R_{min} the size of the smallest particle, $D(R)$ a given size distribution function, and $\alpha_r(R, t)$ given either by Eq. (4) (r ≡ CV) or Eq. (12) (r ≡ D). The initial volume V_0 of the powder is given by

$$V_0=\frac{4}{3}\pi\int_{R_{min}}^{\infty}D(R)R^3\,\mathrm{d}R \tag{25}$$

or alternatively

$$V_0=\frac{W}{\rho} \tag{26}$$

with W the powder's weight and ρ the theoretical density of the powder's material.

The calculated total reacted fraction $\alpha_r^{calc}(t)$ (at time t) of the whole powder is

$$\alpha_r^{calc}(t)=\frac{V_r(t)}{V_0} \tag{27}$$

Substituting different distribution functions $D(R)$ into Eq. (24), and utilizing Eq. (27), the calculated $\alpha_r^{calc}(t)$ vs. t kinetic curves are obtained for any given type of kinetics (r ≡ CV or D).

The corresponding $F_r(\alpha^{calc})$ vs. t curves may then be evaluated and compared with the functional SPA forms given in Eqs. (5) and (9) respectively. The calculations of the integral in Eq. (24) are performed using the trapezoidal method [31]. In the integration procedure, care must be taken to eliminate those particles that have already reacted completely at time t (i.e. $\alpha_i(t)=1$), from further being counted at higher t values. This is done by dividing the integral into

$$V_r(t)=\frac{4}{3}\pi\left(\int_{R_{min}}^{R_r'(t)}D(R)R^3\,\mathrm{d}R+\int_{R_r'(t)}^{\infty}D(R)R^3\alpha_r(R, t)\,\mathrm{d}R\right) \tag{28a}$$

with $R_r'(t)$ given by

$$R_{CV}'(t)=Ut \tag{28b}$$

$$R_D'(t)=(6k_Dt)^{1/2} \tag{28c}$$

As mentioned in Section 2.1, it is convenient to present the kinetic curves $F_r(\alpha)$ on a reduced time scale τ, which for the SPA cases yield for each of the kinetic classes a "universal" slope, related to that class (see Table 1). Such a presentation is thus utilized also

Table 2
Types of distribution functions used in the calculations, and their labelling in the figures

	Distribution functions	
Gaussian	D_G ($\langle R\rangle$, σ; R)	$\begin{cases} 0 & (R<R_{min}) \\ \frac{1}{(2\pi)^{1/2}\sigma}\exp\left(-\frac{(R-\langle R\rangle)^2}{2\sigma^2}\right) & (R\geqslant R_{min}) \end{cases}$
Log-normal	D_{LN} (R_{LN}, σ; R)	$\begin{cases} 0 & (R<R_{min}) \\ \frac{1}{(2\pi)^{1/2}\sigma}\exp\left(-\frac{(\ln R-\ln R_{LN})^2}{2\sigma^2}\right) & (R\geqslant R_{min}) \end{cases}$

Labelling of distribution functions

Function	Labelling in figures
D_G (3, 1; R)	$G1$
D_G (3, 3; R)	$G2$
D_{LN} (3, 0.4; R)	$L1$
D_{LN} (3, 1.2; R)	$L2$

for the different $F_r(\alpha^{calc})$ plotted vs. τ (with $t_{1/2}$ corresponding to $\alpha^{calc}=0.5$). In these calculations a variety of possible distribution functions were applied including symmetric (gaussian) functions, and also asymmetric (log-normal) functions. Table 2 summarizes these applied distributions, which are also shown in Fig. 2. In all cases, R_{min} was set to 1 μm.

The results obtained for the constant-velocity case are presented in Fig. 3 (α_{CV} vs. τ) and Fig. 4 ($F_{CV}(\alpha)$ vs. τ), while the corresponding results obtained for the

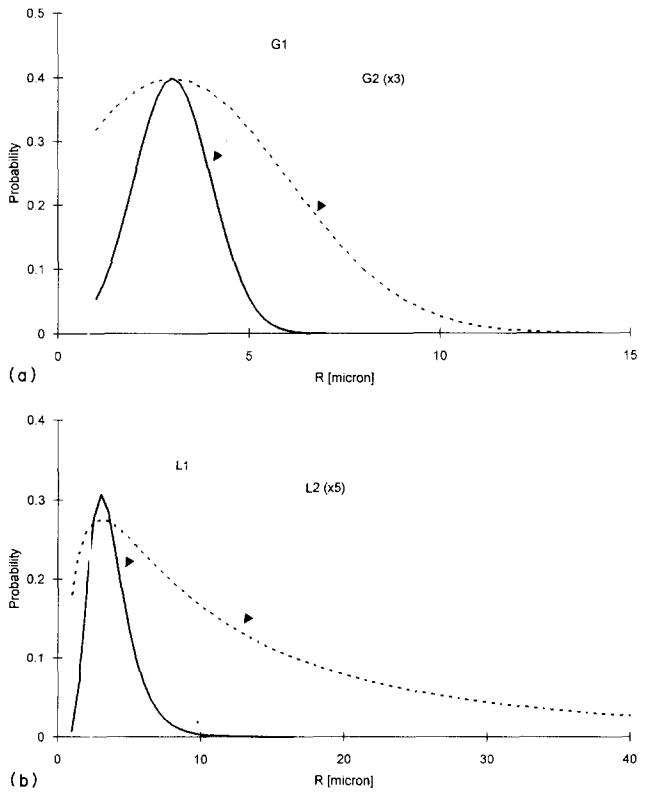

Fig. 2. Different particle size distributions utilized in the calculations (Table 2): (a) Gaussian; (b) log-normal.

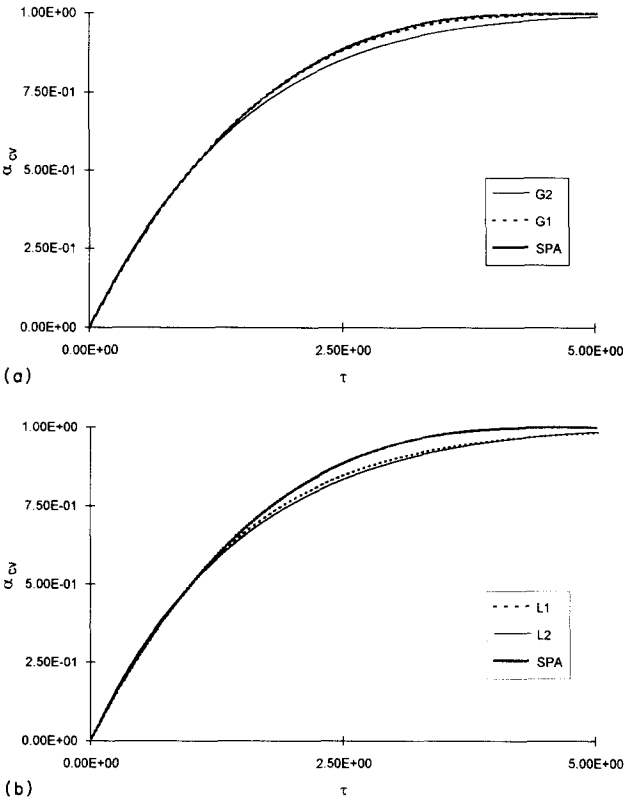

Fig. 3. Effects of size distributions on constant-velocity kinetics of a sphere as shown by calculated reacted fraction α_{CV} vs. reduced time τ curves, for different size distributions (Fig. 2 and Table 2): (a) gaussian distributions; (b) log-normal distributions. The full broad line represents the SPA results.

decelerating velocity diffusion-controlled case are presented in Fig. 5 (α_D vs. τ) and Fig. 6 ($F_D(\alpha)$ vs. τ). It is seen from these figures that the occurrence of a size dispersion leads to some deviations from the linear $F_r(\alpha)$ vs. τ relations. However, these deviations are displayed mainly in the higher α region, whereas a significant region in the lower α range (i.e. up to about $\alpha\approx 0.5$–0.6) displays the linear SPA-like dependence.

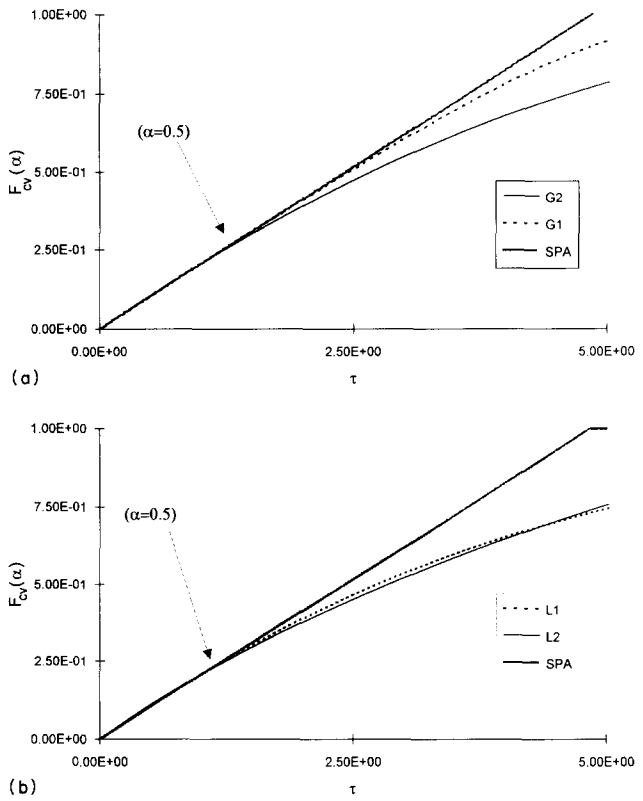

Fig. 4. Effects of size distributions on constant-velocity kinetics of a sphere as shown by calculated reacted fraction function $F_{CV}(\alpha)$ vs. reduced time τ curves for the different size distributions ($\alpha(\tau)$ as obtained in Fig. 3): (a) gaussian distributions; (b) log-normal distributions (the same as in Fig. 3). The full line represents the SPA result.

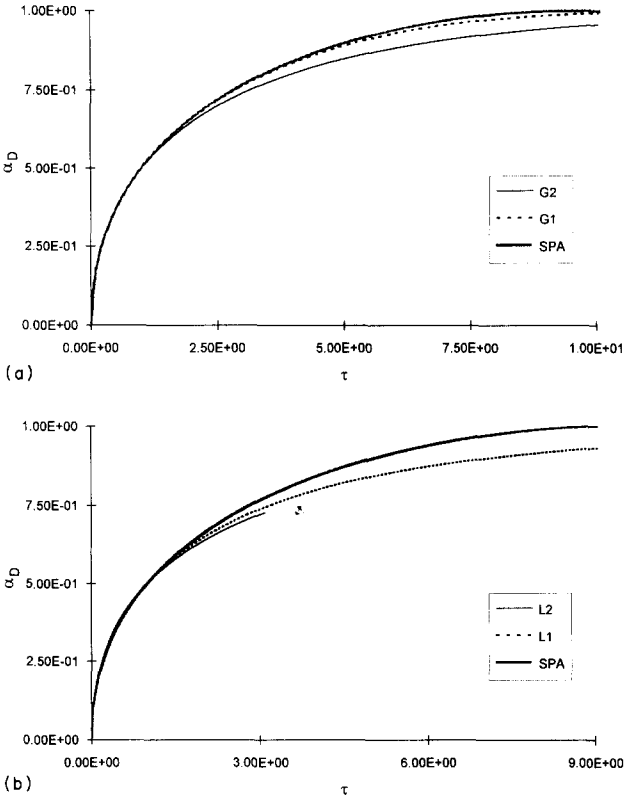

Fig. 5. Effects of size distributions on diffusion-controlled kinetics as shown by α_D vs. τ curves for (a) Gaussian and (b) log-normal distributions (Fig. 2 and Table 2).

Also, the values of the slopes of these linear portions are close to the "universal" SPA values (as listed in Table 1).

Besides those "universal" (i.e. kinetics-type-related) slopes of the $F_r(\alpha)$ vs. τ curves, one can refer also to the system-related slopes of the $F_r(\alpha)$ vs. t curves (i.e. Eqs. (5) and (9)) which depend on the intrinsic kinetic parameters of the reacting sample (i.e. U or k_D respectively) as well as on the size parameter R.

The following questions may then be addressed: is it justified to replace the single-valued parameter R, appearing in the SPA expressions (Eqs. (5) and (9)), by some average $\langle R\rangle$ of the powder? Furthermore, it is known that the conventional average $\langle R\rangle$ is not always the proper quantity to represent integral parameters related to the powder. For example, the material volume and related theoretical density (Eqs. (25) and (26) respectively) are expressed by $\langle R^3\rangle$ rather than by $\langle R\rangle^3$. We may then utilize the more generalized form for the average moment of order n:

$$\langle R_n\rangle = \left(\int_{R_{min}}^{\infty} D(R)R^n\,dR\right)^{1/n} \tag{29}$$

with $n=1, 2, 3,\ldots$ (i.e. $n=1$ corresponds to the conventional average) and check the validity of these $\langle R_n\rangle$ substitutions into the SPA expressions. In these calculations, some arbitrary value of either U (in Eq. (5)) or k_D (in Eq. (9)) were chosen. The corresponding $\langle R_n\rangle$ ($n=1, 2, \ldots$) values are evaluated, for any given size distribution (utilizing Eq. (29)), and the corresponding SPA-like slopes are then obtained (i.e. $U/\langle R_n\rangle$ for constant-velocity kinetics and $2k_D/\langle R_n\rangle^2$ for diffusion-controlled kinetics). These slopes are compared with the respective initial slopes in the linear region of $F_r(\alpha^{calc})$ vs. t curves (α^{calc} evaluated by Eq. (27)). The ratios of the SPA-like slopes (for the given $\langle R_n\rangle$) to the calculated $\partial F_r(\alpha^{calc})/\partial t$ slopes are summarized in Table 3. It should be pointed out that, even though the specific choice of a given intrinsic kinetic parameter (i.e. U or k_D) affects the absolute values of the corresponding slopes, the above-mentioned slope ratios are insensitive to that choice, yielding similar results. It turns out from Table 3 that, for a given intrinsic kinetic parameter, utilization of the average moments of the order of about 5–6 best fits the initial linear slopes obtained from the $F_r(\alpha)$ vs. t curves. For example, utilizing $\langle R_5\rangle$, the maximum deviation of the SPA-like slope from the "real" slope is about 30%, with most of the deviations ranging within $\pm 20\%$. Hence, performing the kinetic analysis of a given powder,

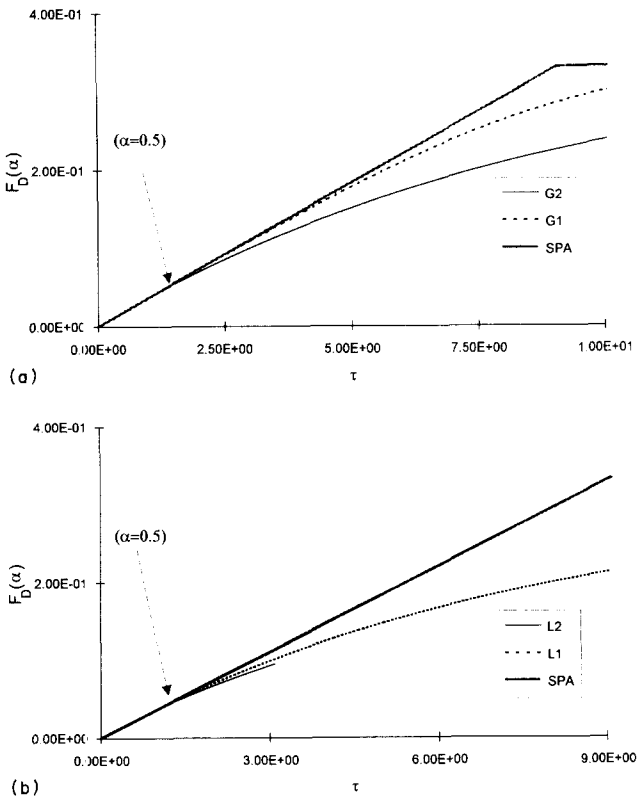

Fig. 6. Effects of size distributions on diffusion-controlled kinetics as shown by $F_D(\alpha)$ vs. τ curves for (a) Gaussian and (b) log-normal distributions (with $\alpha_D(\tau)$ as obtained in Fig. 5).

Table 3
Typical ratios of SPA-like slopes (i.e. $U/\langle R_n\rangle$ and $2k_D/\langle R_n\rangle^2$ as appearing in Eqs. (5) and (9) respectively, for the different mechanisms) to the corresponding $\partial F_r(\alpha^{calc})/\partial t$ initial linear slopes, for any given particles size distribution, the $\langle R_n\rangle$ values in the SPA-like slopes were calculated (according to Eq. (29)), with $n=1$–8

Type of kinetics	Distribution function D (R)	Ratio of SPA-like slopes to the calculated $\partial F_r(\alpha^{calc})/\partial t$ slopes, using the different moments, $\langle R_n\rangle$ with the following n values							
		1	2	3	4	5	6	7	8
r≡CV	G1	1.23	1.16	1.11	1.07	1.04	1.00	0.98	0.95
	G2	2.02	1.56	1.35	1.22	1.12	1.05	1.00	0.95
	L1	1.40	1.29	1.19	1.10	1.02	0.95	0.88	0.82
	L2	4.10	2.33	1.54	1.15	0.93	0.79	0.70	0.64
r≡D	G1	1.53	1.36	1.25	1.16	1.08	1.02	0.97	0.92
	G2	4.12	2.45	1.84	1.50	1.28	1.12	1.00	0.90
	L1	1.96	1.67	1.43	1.22	1.05	0.91	0.79	0.69
	L2	16.1	5.26	2.29	1.27	0.83	0.61	0.48	0.40

i.e. fitting a linear $F_r(\alpha)$ vs. t dependence, which yields the corresponding initial linear slope $\partial F_r(\alpha)/\partial t$, enables not only the identification of the controlling mechanism (i.e. r≡CV or D) but also the reasonable estimation of the corresponding intrinsic kinetic parameters (i.e. U in Eq. (5) or k_D in Eq. (9)), which are approximated by

$$U \approx \langle R_5\rangle \left.\frac{\partial F_{CV}(\alpha)}{\partial t}\right|_{t<t1/2} \tag{30}$$

$$k_D \approx \frac{1}{2}\langle R_5\rangle^2 \left.\frac{\partial F_D(\alpha)}{\partial t}\right|_{t<t1/2} \tag{31}$$

with $\langle R_5\rangle$ calculated from the known size distribution of the powder utilizing Eq. (29).

2.2.2. Effects of shape variations

It is clear that the assumption of perfect spherical particles composing the powder is a crude simplified description for most powders. It is therefore necessary to have some estimation of the effects of shape variations on the kinetic analysis presented before. Like the questions addressed in the size distributions analysis, two categories of effects should be evaluated, namely effects on the "universal" mechanistic-related curves (i.e. plotted on a reduced time scale τ, (Eq. (15))), and effects on the system-related curves (involving slopes related to the intrinsic kinetic parameters) plotted on a regular time scale t.

In order to estimate the former effect, the SPA expressions for different geometrical shapes can be used. Choosing two shapes which significantly differ from a sphere, namely a wire (radius R; length L; $L \gg R$) and a disk (radius R; height H; $R \gg H$), the following kinetic functions for the constant-velocity progression can be applied: for a disk,

$$F_{CV,d}(\alpha) = \alpha = \frac{2U}{H}t \tag{32}$$

and, for a wire,

$$F_{CV,w}(\alpha) = 1-(1-\alpha)^{1/2} = \frac{U}{R}t \tag{33}$$

with the subscripts d and w denoting the respective geometries.

For a reduced time scale (Eqs. (15) and (17)) the above expressions assume the "universal forms"

$$F_{CV,d}(\alpha) = \alpha = F_{CV,d}(0.5)\tau = 0.50\tau \tag{34}$$

$$F_{CV,w}(\alpha) = 1-(1-\alpha)^{1/2} = F_{CV,w}(0.5)\tau = 0.29\tau \tag{35}$$

whereas, for spherical geometry, $F_{CV,s}(\alpha)$ is given by Eq. (5) and its "universal" slope on the reduced time scale is 0.21 (Table 1). Now consider the case of a wire, reacting according to Eqs. (33) and (35) and yielding a certain experimental $\alpha_w^{exp}(t)$ kinetics. However, assume that these results are inadvertently analyzed according to the spherical expression $F_{CV,s}(\alpha)$, utilizing the reduced time presentation. According to Eq. (35), the "experimental" τ dependence is

$$\alpha_w^{exp}(\tau) = 1-(1-0.29\tau)^2 \tag{36}$$

If this expression, however, is "mistakenly" substituted into the spherical case, i.e.

$$F_{CV,s}(\alpha_w^{exp}) = 1-(1-\alpha_w^{exp})^{1/3} \quad (37)$$

the resulting $F_{CV,s}$ (α_w^{exp}) vs. τ curve is illustrated in Fig. 7. It is seen that the linear dependence is still maintained over most of the α_w^{exp} range. The linear slope can be calculated from

$$\frac{\partial F_{CV,s}(\alpha_w^{exp})}{\partial \tau} = \frac{\partial F_{CV,s}(\alpha_w^{exp})}{\partial \alpha_w^{exp}} \frac{\partial \alpha_w^{exp}}{\partial \tau} \quad (38)$$

which, by utilizing Eq. (37) and Eq. (36), yields

$$\frac{\partial F_{CV,s}(\alpha_w^{exp})}{\partial \tau} = \frac{2\times 0.29}{3}(1-0.29\tau)^{-1/3} \quad (39)$$

For $\tau < 1$, the initial slope is then approximately 0.19, which is close to the value of 0.21 obtained for the "real" spherical case.

A similar analysis can be done for the disk (Eq. (34)). Here, substituting the "experimental" α_d^{exp} into the spherical expression

$$F_{CV,s}(\alpha_d^{exp}) = 1-(1-0.5\tau)^{1/3} \quad (40)$$

yields a curve which again, up to about $\tau \approx 1$ (i.e. $\alpha_d^{exp} \approx 0.5$) is linear (Fig. 7), with a slope of about 0.17, again not much different from the "real" spherical case.

It can easily be shown that, also for diffusion-controlled kinetics, substitution of the disk (i.e. planar) expression

$$\alpha_d^{exp} = 0.5\tau^{1/2} \quad (41)$$

into the spherical $F_{d,s}(\alpha)$ vs. τ function (Eq. (9)) yields a curve which is almost linear up to about $\alpha \approx 0.5$ with a slope of about 0.028, close to the value of 0.037 obtained for real spherical symmetry (Table 1).

It is thus concluded that, for the contracting-envelope kinetic functions, the variations in the "universal" forms

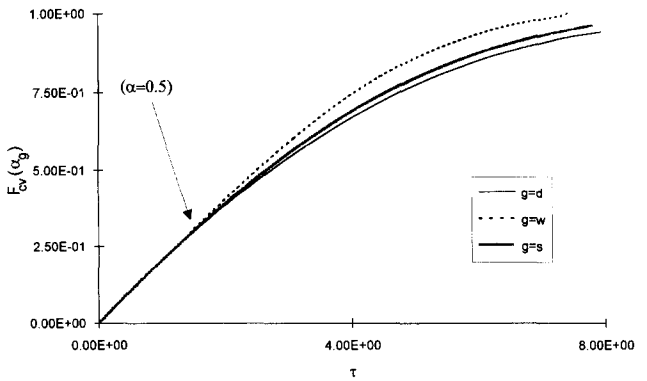

Fig. 7. Effects of shape variations on the constant-velocity kinetics (plotted on a "universal" reduced time scale). The ordinate represents $F_{CV,s}$ (α_g^{exp}), the spherical function (Table 1), in which α_g^{exp} values of reacting non-spherical particles (g≡wire or disc respectively) were substituted and compared with the spherical case.

(and "universal" slopes) of these functions, induced by geometrical shape changes, are much less pronounced than the variations induced by changes in the controlling mechanism (i.e. r≡CV or D). Hence, applying the $F_{r,s}(\alpha)$ vs. τ analysis, utilizing the spherical-geometry expression, is still valid for non-spherical geometries which, even though they result in some deviations from linearity at higher α values, still display a linear dependence (for the correct mechanism) over a relatively wide range of α, with the "universal" linear slope indicative of the respective mechanism. In other words, variations in particle shape do not alter much of the above analysis, which properly points to the controlling mechanism.

The second issue that should be considered now is the ability to obtain the respective intrinsic kinetic parameters (i.e. U or k_D) from the linear regions of the $F_{r,s}(\alpha)$ vs. t curves, for powders with non-spherical particles. In this case, expressions of the type given by Eq. (30) (for constant-velocity kinetics) or Eq. (31) (for diffusion-controlled kinetics) should be used, but with some "effective" spherical radius R^e replacing the defined spherical case. The question to be addressed then regards the type of "effective" radius which should be utilized and to what accuracy does it yield the respective intrinsic kinetic parameters.

For constant-velocity kinetics, comparing the initial $F_{CV,s}(\alpha \ll 1)$ time dependence expressed by Eq. (5′) with the corresponding planar case [14]

$$\alpha_{CV,p}(t) = \frac{2U}{H}t \quad (42)$$

(with H being the thickness of the planar sample) it turns out that choosing the smallest dimension of the planar sample as the "effective radius" (i.e. $R^e = H$) and substituting the correct $\alpha_{CV,p}^{exp}$ kinetics (Eq. (42)) into the spherical $F_{CV,s}(\alpha \ll 1)$ case (Eq. (5′)), the resulting error in U is about 30% (since the "real", i.e. "experimental", slope is then $2U/3R^e$ whereas the effective assumed slope is U/R^e). A better choice for an "effective" radius would thus be $R^e = \frac{3}{2}H$, which then leads to the exact U value.

A more generalized analysis can be presented for a non-spherical particle with a given λ_a axial ratio (or aspect ratio). Assume a cylinder, with a radius R_c and a height H_c reacting according to the constant-velocity kinetics. The reacted fraction time dependence is then given by (in [14] a similar expression is given but with an error in the quadratic term coefficient, which is corrected in Eq. (43))

$$\alpha_{CV,c}(t) = 2\left(\frac{1}{H_c}+\frac{1}{R_c}\right)Ut - 4\left(\frac{1}{R_cH_c}+\frac{1}{R_c^2}\right)(Ut)^2 + \left(\frac{2}{H_cR_c}\right)(Ut)^3 \quad (43)$$

Defining the axial ratio

$$\lambda_a = \frac{2R_c}{H_c} \tag{44}$$

Eq. (43) can be rewritten as

$$\alpha_{CV,c} = \frac{\lambda_a + 2}{R_c} Ut - \frac{2(\lambda_a + 2)}{R_c^2} \times (Ut)^2 + \frac{\lambda_a}{R_c^3} (Ut)^3 \tag{45}$$

However, assuming a "spherical-equivalent" particle with effective radius R^e reacting according to Eq. (4) (with R^e replacing R), equating the two linear-term coefficients in these expressions yields the best choice for R^e as

$$R^e = \frac{3}{\lambda_a + 2} R_c \tag{46}$$

(Note that this expression is different from the volume-equivalent spherical radius given by $(3/2\lambda_a)^{1/3}R_c$.) Some specific cases derived from Eq. (46) are as follows: (i) symmetric cylinder, $\lambda_a = 1$, for which $R^e = R_c$; (ii) wire-like geometry, $\lambda_a \ll 1$, for which $R^e \approx 1.5R_w$ (R_w is the wire radius); (iii) plate-like geometry, $\lambda_a \gg 1$, for which $R^e \approx 1.5H_p$ (H_p is the height of the plate), as discussed above. Hence, for very asymmetric particles, the effective spherical radius is related to the smallest dimension of the corresponding shape. Similarly, for diffusion-controlled kinetics, comparing the initial $F_{D,s}$ ($\alpha \ll 1$) time dependence presented by Eq. (9′) with the planar case [14] (neglecting the volume change associated with product formation, $\epsilon \to 1$), i.e.

$$\alpha_{D,p}^2(t) = \frac{8k_D}{H^2} t \tag{47}$$

and substituting into Eq. (9′) $R^e = H$ lead to an error of a factor of $18/8 = 2.25$ in the calculated value of k_D. This error is much larger than the error of about 30% obtained for the corresponding constant-velocity kinetics. Hence, the best choice for R^e in this case would be

$$R^e = \left(\frac{18}{8}\right)^{1/2} H = 1.5H \tag{48}$$

which is the same best substitution obtained for constant velocity kinetics. To conclude this part it can thus be assumed that, for powders characterized by non-spherical but still shape-defined particles, utilizing Eq. (30) or (31), with $\langle R_5^e \rangle$ replacing $\langle R_5 \rangle$, will yield a relatively accurate estimate of the intrinsic kinetic parameters. In a gross manner, for very asymmetric particles, denoting the smallest dimension of the corresponding shapes by δ (e.g. $\delta = H$ for disks, and $\delta = R_w$ for wires), then

$$\langle R_5^e \rangle \approx 1.5 \langle \delta_5 \rangle \tag{49}$$

(with $\langle \delta_5 \rangle$ defined by an equation similar to Eq. (29)) whereas symmetric particles are characterized by a single spherical-equivalent dimension A (of about a radius of a sphere enclosed within the corresponding shape) with

$$\langle R_5^e \rangle = \langle A_5 \rangle \tag{50}$$

However, for powders with a wide dispersion of shapes(e.g. containing both asymmetric and symmetric particles), the choice of $\langle R_5^e \rangle$ is more complicated and, even though the corresponding controlling kinetics (i.e. constant velocity or diffusion controlled) can be evaluated (by $F_{r,s}(\alpha)$ vs. τ analysis), accurate estimation of the intrinsic kinetic parameters is not possible.

2.2.3. Effects of initiation time distributions

In Sections 2.2.1 and 2.2.2, it was assumed that the commencement of the reaction occurs instantaneously on all powder's particles. In fact, different particles may start to react at different times, leading to a spread of these initiation times. In order to evaluate the effects of such time dispersions on the SPA-like procedure, a Monte Carlo procedure was utilized to "activate" randomly any given particle in the powder (with a given size distribution function). A "marker" parameter $0 \leqslant M \leqslant 1$ was defined for each computer run. Then, for a given reaction time t, a scan over all particles was made. For a given individual particle i, a random number $0 < P_i \leqslant 1$ was generated with the condition that, if $P_i \leqslant M$, the specific particle is "activated" (i.e. starts to react at the given time t) whereas, if $P_i > M$, the particle does not react at this time. Any particle which had started to react at a time $t' \leqslant t$ was assumed to follow the kinetics presented by Eq. (21), with $t - t'$ replacing t. For a given intrinsic kinetic parameter (i.e. either U or k_D), summing α_i over all reacting particles yielded the corresponding $\alpha(t)$ value. Then, the reaction time was increased by some increment Δt, and the above procedure repeated. In this way, the $\alpha(t)$ vs. t dependence was computed, for any given size distribution, and kinetics (i.e. constant velocity or diffusion controlled).

It is evident that, as M approaches unity, the distribution function of initiation times narrows (with $M = 1$ corresponding to the instantaneous commencement case).

Fig. 8(a) presents the initiation time distributions $N(t)$ obtained for a given ensemble (of 20 000 particles), for different choices of M. These distributions are gaussian like with a maximum at $t = 0$ (i.e. no induction period is assumed for the first reacting particles) and a width $\sigma_t(M)$, which broadens as M decreases. The corresponding $\alpha(t)$ vs. t curves (for the different $N(t)$ distributions) were calculated for a given size distri-

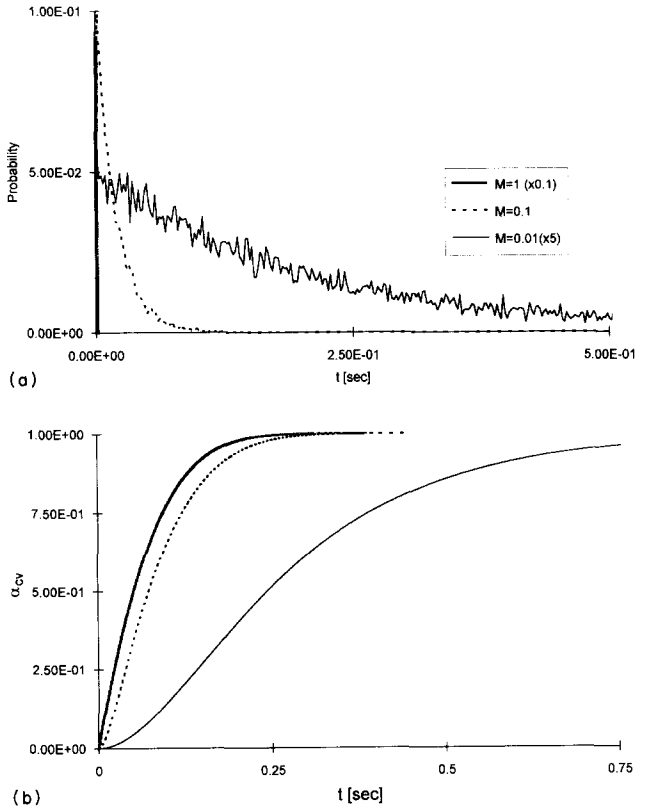

Fig. 8. (a) Probability distribution of number of particles which start to react at time t, for different choices of the "marker" parameter M (see text). The widths σ_t of these distributions corresponding to the different M values are as follows: $M=1$, $\sigma_t=0$; $M=0.1$, $\sigma_t=1.3\times10^{-3}$ s; $M=0.05$, $\sigma_t=0.13$ s. (b) Effects of initiation time distributions (as displayed in (a) on the α_{CV} vs. t kinetic curves. Labelling as in (a).

bution function ($G2$ in table 3), assuming constant-velocity kinetics and some given U values (which determine $t_{1/2}$). Fig. 8(b) summarizes the corresponding α vs. t behaviour, displayed for different σ_t values. Two effects are apparent from these kinetic curves: (i) a displacement of $t_{1/2}$ towards higher values resulted by the delay in the commencement of the reaction for some of the particles; (ii) inflection points introduced into the curves, which now assume an S-like shape. This behaviour qualitatively resembles the nucleation-and-growth kinetics (i.e. Eq. (13)); however, the inflection points in the latter case are located at about $t\approx t_{1/2}$ (cf. Eq. (20)) whereas, for the present kinetics, inflection occurs at $t\ll t_{1/2}$.

The modification of the kinetic behavior by such initiation time distributions may thus obliterate the mechanistic-related functional dependences, leading to a situation where the SPA procedure cannot be applied to the powder. This situation is encountered when the σ_t values (i.e. time distributions widths) are comparable with the intrinsic $t_{1/2}$ values of the reaction (i.e. the $t_{1/2}$ values obtained for the case when all particles start to react simultaneously).

3. Discussion

The present analysis demonstrates that under certain circumstances the kinetic measurements performed on powders can be interpreted by applying the SPA procedure. Besides the extrinsic experimental parameters (e.g. an effective heat and mass conduction) which should be carefully controlled, and which pose a certain technological difficulty in such measurements [7,9–13], there are some intrinsic kinetic factors which may exclude the application of the above SPA. The two main factors of this category are (1) dispersed time distributions for the commencement of the reaction on the different particles composing the powder (as has been discussed in Section 2.2.3) and (2) a relatively fine size of powder particles, ranging within the magnitude of X_0 (Eq. (2)), i.e. the initial thickness of the continuous product film developing on the surface. In this conjunction, it should be realized that, since repeated hydriding–dehydriding cycles initially result in particulation of the material into finer particles (up to a certain extent attained after a given number of cycles), it is possible that the overall kinetics displayed for consecutive hydriding–dehydriding experiments may change. Starting with a powder with relatively coarse particles (i.e. such that $X_0/\langle R\rangle \ll 1$) the dominant kinetics then follow the contracting envelope SPA functions (i.e. Eqs. (4) and (5) or Eqs. (9) and (12)). However, if the size distribution of that powder shifts into smaller $\langle R\rangle$ values by repeated cycling, leading to a situation when $X_0/\langle R\rangle \approx 1$, then the former contracting-envelope kinetics are obliterated. In the extreme case ($X_0/\langle R\rangle \geqslant 1$) S-shaped kinetics related to nucleation-and-growth mechanisms (Eq. (13)) are taking place.

On the contrary, the effects of size distributions as well as shape variations are usually not drastic enough to prevent the identification of the proper type of kinetics by the SPA procedure. In addition to the evaluation of the controlling kinetics, it is important to obtain the numerical values of the corresponding intrinsic kinetic parameters (e.g. U for constant-velocity kinetics or k_D for diffusion-controlled kinetics), as well as their pressure–temperature dependence [14]. In this context it has been shown in the present analysis that for nearly symmetrical particle shapes, regardless of the size distribution of the powder, a relatively accurate estimate of these parameters is possible (Eq. (30) or (31)), if the particular size distribution function of the reacting sample is known. For asymmetrical particles (e.g. platelet-like shapes and wire-like particles) a more complex analysis is required (e.g. Eq. (49)), utilizing averaged parameters related to the smallest dimension of the corresponding particle shape. However, in these cases the accuracy in the absolute values of the intrinsic kinetic parameters is less than in the case of symmetric particles. It should further be noted that unlike the

determination of the absolute values of intrinsic kinetic parameters (at a given pressure and temperature) the accurate evaluation of apparent "activation energies" E_a associated with these parameters [14] is possible even for unknown size distributions or shape factors of the powders. As long as the functional form of the SPA kinetics (e.g. Eq. (3)) is established (which does not require knowledge of these distributions), a parameter $k(T)/\langle R_n\rangle^m$ is evaluated, with $k(T)$ being proportional to the (temperature-dependent) intrinsic kinetic parameter, and $\langle R_n\rangle^m$ a dimension-related factor (e.g. $\langle R_5\rangle$ or $\langle R_5\rangle^2$ in Eq. (30) or (31) respectively). Hence, even when $\langle R_n\rangle^m$ is not known, still an Arrhenius plot of $\ln[k(T)/\langle R_n\rangle^m]$ vs. $1/T$ will yield the apparent E_a, if the corresponding intrinsic kinetic parameter does obey such an Arrhenius dependence. This consideration has been pointed out previously by Kapur [25], although in a somewhat different way. In fact, the procedure outlined there [25] enables the determination of E_a even without the evaluation of the specific functional form of the kinetic data (i.e. without the choice of a particular $F_{r,g}(\alpha)$ in Eq. (3)).

The above considerations about the evaluation of E_a should be modified to some extent when analysing kinetic experiments performed under conditions which are close to equilibrium, i.e. under such working pressures P and temperatures T, where P is not very much different from $P_e(T)$ (the equilibrium plateau pressure of the hydride). In these cases the intrinsic kinetic parameters (or the related k rate constants) are modified by temperature variations in a complex way owing to the simultaneous interplay of the formation and decomposition processes. The typical Arrhenius dependence attained under far-equilibrium conditions is then replaced by a complex temperature behaviour, displaying a maximum in the ln k vs. $1/T$ curves [14]. Hence, the evaluation of E_a requires knowledge of the pressure dependence of $k[P, P_e(T), T]$. Otherwise, different E_a values can be assigned for different possible $k[P, P_e(T)]$ relations [7,9], with no real physical significance of these "activation" parameters.

It is worthwhile to demonstrate some qualitative trends emerging from the present analysis which may account for some controversial kinetic results reported in the literature. One example concerns the kinetics of formation of the $LaNi_5$–H_2 system (actually the $LaNi_{4.9}Al_{0.1}$ alloy) as reported in two publications [7,9]. In these studies, two types of kinetics are reported, one [9] corresponding ot the contracting-envelope kinetics (Eq. (5)), and the other [7] corresponding to bulk nucleation and growth (Eq. (14)) with $n=2$. In both studies the applied experimental conditions (P and T) were in the same range, and care has been taken to keep isothermal–isobaric control during the kinetic measurements.

According to the above discussion, two possible factors could account for the change in the observed kinetics. One factor is the occurrence of a significant spread (distribution) in the times of commencement of the reaction (on each of the powder's particles), whereas the second possible factor is an increase in the $X_0/\langle R\rangle$ ratio.

As for the former possibility, it has been pointed out in Section 2.2.3 that such a time distribution may lead on the one hand to a significant increase in $t_{1/2}$ (i.e. slower kinetics) and on the other hand to the appearance of inflection points in the α vs. t kinetic curves, similar to nucleation-and-growth kinetics. It is evident that both symptoms are apparent in the data presented in [7]. Different reasons may be postulated for the existence of such an effect. One possibility is the presence of some gas-phase impurities which inhibit to some extent the hydriding reactions, leading to the dispersed initiation time distribution. The samples size utilized in [7] are about three orders of magnitude smaller than those used in [9] (only 5 mg in the former compared with about 5 g in the latter). It is thus possible that chemisorption of such minor impurities on the (large) surface area of the larger samples [9] inhibits only a small and insignificant fraction of the powder, whereas for the smaller samples [7] such inhibition effects are pronounced. There is, however, one point which may cast doubt on the above reasoning. The location of the inflection point in the data presented in [7] is at about $\alpha\approx 0.5$ (i.e. $t\approx t_{1/2}$). As discussed before, inflection points induced by dispersed commencement time distributions are usually located at $\alpha \ll 0.5$, which is inconsistent with these experimental results.

As for the second possibility mentioned above, i.e. an increase in the $X_0/\langle R\rangle$ ratio, such an increase may be the result of two factors; it could be due either to a decrease in $\langle R\rangle$ (i.e. a finer powder with smaller particles) or to an increase in X_0 (i.e. the completion of a continuous product layer covering the surface, occurring at a larger α value, for a given size distribution). No experimental details on the size distributions of the powders utilized in [7,9] were presented. However, since in both studies the samples were activated by several hydriding–dehydriding cycles, it is not likely that these size distributions could differ by such an extent as to account for the observed change in kinetics. Moreover, the $t_{1/2}$ values obtained in [7] are much higher then those in [9] (under similar conditions). If the reason for the change into nucleation-and-growth kinetics was attributed to a finer particle size distribution (in [7]), then the opposite trend (i.e. faster kinetics, or shorter $t_{1/2}$ values) would be anticipated. Hence, this possible explanation can be ruled out.

The other alternative for an increase in the $X_0/\langle R\rangle$ ratio is, as mentioned above, an increase in X_0, occurring

under the experimental conditions applied in [7]. It is illustrated in Fig. 1 that the preceding stage to the formation of a continuous product layer on the surface of a given reacting particle involves a nucleation-and-growth process. Hence, for a given nuclei growth rate, it is anticipated that a lower nucleation density will result in a larger X_0 value (since the complete overlap between the growing nuclei is then delayed to larger X_0). Since the nucleation density is very sensitive to the presence of gas-phase impurities [32], the reasoning presented above (i.e. smaller samples utilized in [7] which are more prone to the effects of impurities) is relevant also for the present case. This explanation is also consistent with the increase in the $t_{1/2}$ values observed in [7]. Hence, the differences between the results reported in the two above publications are reasonably accounted for by the increase in X_0 due to a lower nucleation density under the conditions applied in [7].

Another example, illustrating the effects anticipated for the case of a time distribution for the commencement of the reaction on the different particles, is given by the data presented in a recent publication on the hydriding kinetics of $LaNi_{5-x}Al_x$ alloys [33]. According to this study, increasing the aluminium content of the alloy (i.e. increasing x) results in a shift in $t_{1/2}$ towards higher values, concomitant with an inflection point (in the α vs. t curves) occurring at low α values. This is similar to the behaviour displayed in Fig. 8(b). Such behaviour has not been analysed by Zhang *et al.* [33] and can be accounted for by the present considerations.

Finally, it should be pointed out that the present analysis is relevant not only to the case of powders but also to some topochemical forms displayed during the hydriding reactions of massive polycrystalline samples. In certain cases [34,35], metallographic examinations of partially hydrided samples have revealed that the reaction progresses by fast diffusion of hydrogen along grain boundaries, and the formation of a product hydride layer coating each of the grains in the sample, developing from the outer grain boundary inside the grain. Hence, even though a bulk (non-powdered) sample is concerned, the overall kinetics resemble the contracting-envelope kinetics of a powder, with grain size distributions replacing the particles size distributions in the powder. A similar situation has been observed for the hydriding of bulk $LaNi_5$ [36], where the reaction commences along preferred bulk paths (probably grain boundaries or microcracks), resulting in the particulation of the bulk sample at a very early stage (i.e. a very small α) of the reaction. A detailed discussion of these measurements will be presented elsewhere [36]. It is, however, important to recall that in such cases some confusion may arise when attempting to analyse the kinetic data, without noting the particular topology of product progression. Assume that such a polycrystalline bulk sample, with a well-defined initial geometrical shape (e.g. a cube with an edge size $A \times A \times A$), yields a certain experimental α vs. t kinetic curve, which actually corresponds to the above-mentioned topochemistry (i.e. contracting-envelope constant-velocity kinetics developing on each of the grains in the bulk sample). However, without noticing the case, the α vs. t data are fitted to the SPA functions (Eq. (4) or (5)) assuming a real single-particle reaction (i.e. assuming that the sample reacts by conventional contracting-envelope constant-velocity kinetics, with the product developing on the surface of the cube and progressing inwards). Evidently, in both cases the SPA functions (4) or (5) will yield a very good fit to the α vs. t curves. In the former (real) case, however, $\langle R_5 \rangle$ (averaged over the grain size distribution) should be substituted, according to Eq. (30), leading to the correct value of U, whereas for the latter (mistaken) case the cube dimension A is utilized, leading to an erroneous estimation of U. This type of incorrect analysis can be prevented by either performing metallographic observations on partially hydrided samples (noting then the real morphological form of product development), or alternatively by performing the SPA procedure on different sizes of samples (e.g. a set of cubes with increasing dimensions). For a conventional SPA case (contracting envelope following the geometrical shape of the sample), the slopes of the $F_{CV}(\alpha)$ vs. t curves (Eq. (5)) should decrease with increasing A value, whereas for the grain-boundary constant-velocity case the same slopes ($U/\langle R_5 \rangle$) should be displayed regardless of the initial dimensions (or shape) of the reacting sample. Hence, such a size (or shape) analysis simply identifies the correct morphological characteristics of product development.

4. Conclusions

The validity in utilizing spherical SPA models for the interpretation of kinetic data obtained for gas–solid reactions (e.g. hydriding reactions) performed on powders was evaluated. The SPA models discussed included two types of contracting-envelope kinetics (cf. Fig. 1): one with a constant-velocity interface movement and the other with a decelerating diffusion-controlled boundary progression. The corresponding SPA kinetic functions for a spherical geometry are given by Eqs. (4) and (5) or by Eqs. (9) and (12) respectively. These types of functions are conventionally applied in the literature to interpret the kinetics of powders. The justification for such a procedure is not a priori straightforward because of three factors inherent in powder kinetics which may modify the spherical SPA behaviour. These factors are (i) particle size distributions, (ii) particle shape variations and (iii) time distributions for

the commencement of the reaction on each of the particles composing the powder.

In the present work, the effects of these powder-inherent factors are quantitatively analysed and their interference in the SPA procedure is estimated. The outcome of this analysis refers to two main questions.

(1) Can the SPA analysis yield the correct type of kinetics controlling the gas–solid reaction of the powder, i.e. can it identify correctly either the constant-velocity or the diffusion-controlled kinetics?

(2) Beyond the identification of the type of kinetics, is it possible to obtain by such an analysis a quantitative estimate of the associated intrinsic kinetic parameter [14], i.e. to evaluate U or k_d in Eqs. (4) and (5) or Eqs. (9) and (12) respectively?

The conclusions obtained, regarding the questions addressed above, are as follows.

(1) As long as all the particles composing the powder start to react simultaneously (or at least when the time spread for the commencement of the reaction on each of the particles is much smaller than the reaction half-time $t_{1/2}$), and as long as a continuous product layer is formed on each particle at a very early stage (i.e. X_0 in Eq. (2), illustrated in Fig. 1, is much smaller than the dimensions of the reacting particles), the occurrence of either dispersed size distributions of particles or particle shape variations (from spherical symmetry) does not lead to significant deviations from the spherical SPA functions, over a relatively wide range of the reaction course (i.e. up to $\alpha \approx 0.5$–0.6). This is displayed in Figs. 3 and 4 for the constant-velocity kinetics, and in Figs. 5 and 6 for the diffusion-controlled kinetics. Hence, the correct identification of the controlling type of kinetics (i.e. either constant velocity or diffusion controlled) is possible in these cases, even without knowledge of the specific size distribution function of the powder, or its particle shapes.

(2) The controlling type of kinetics mentioned above can be identified by checking the $F_{r,g}(\alpha)$ time behaviour (Eq. (3)) with g corresponding to the spherical geometry (or any other chosen geometry which in fact is not significant for that purpose) and r corresponding either to constant-velocity kinetics (Eq. (5)) or diffusion-controlled kinetics (Eq. (9)). The substitution of the experimental $\alpha(t)$ data into the $F_{r,g}(\alpha)$ vs. t curve should yield an initial linear dependence for the correct type of controlling kinetics (linearly up to about $\alpha \approx 0.5$–0.6).

Alternatively, presenting the $F_{r,g}(\alpha)$ vs. reduced time scale ($\tau = t/t_{1/2}$) should yield for the proper kinetics a linear dependence (up to $\tau \approx 1$), with a "universal slope" typical of the type of kinetics (see Table 1). Hence, the difference between these two alternatives of data analysis is that, while the former type of presentation (i.e. $F_{r,g}(\alpha)$ vs. t curves) yields (for the given proper kinetics) linear slopes which depend on the experimental pressure–temperature conditions (because of the dependence of the corresponding intrinsic kinetic parameters [14]), the latter (i.e. $F_{r,g}(\alpha)$ vs. τ) presentation yields a fixed slope (for all the applied pressure–temperature conditions) typical of the type of kinetics only.

(3) Besides identification of the controlling kinetics, since the initial linear slopes (obtained for the proper kinetics) of the $F_{r,g}(\alpha)$ vs. t curves are proportional to the corresponding intrinsic kinetic parameters, it is possible to evaluate by this analysis the functional temperature and pressure dependences of these kinetic parameters (although not their absolute values). For example, Arrhenius plots of these linear slopes can yield the apparent activation energies. (For hydriding reactions, especially for non-stable intermetallic hydrides, special considerations of the Arrhenius-type plots should be made when approaching near-equilibrium conditions, as mentioned in the discussion part of this article). Hence, qualitative pressure–temperature trends and apparent activation energies can also be evaluated in these cases without knowledge of either particle size distributions or particle shapes.

(4) In order to evaluate the absolute values of the associated intrinsic kinetic parameters (i.e. U for constant-velocity kinetics and k_d for diffusion-controlled kinetics), it is necessary to determine the shapes and the size distributions of the powders. The accuracies of such absolute values estimations depend on the shape variations of the particles in the powders.

(i) For powders composed of nearly axially symmetric particles (e.g. nearly spherical, nearly cubic and symmetric polyhedra), accuracies better than $\pm 30\%$ can be obtained, utilizing Eq. (30) or Eq. (31) for constant-velocity or diffusion-controlled kinetics respectively.

(ii) For powders composed of axially asymmetric particles (e.g. platelets and wire-like particles) but uniformly shaped, averaging is made over the smallest dimension of the corresponding shape (e.g. the radius of the wire), and Eq. (49) replaces the axially symmetric average moment (i.e. $\langle R_5 \rangle$) in Eqs. (30) and (31).

(iii) For powders composed of particles with variable shapes (i.e. including both axially symmetric and axially asymmetric particles), the estimation of the absolute values of the intrinsic kinetic parameters is not accurate, and only identification of the type of controlling kinetics and qualitative pressure–temperature trends (as summarized in conclusions (1)–(3)) are applicable.

(5) For cases when the time spread for the initiation of the reaction on each of the particles composing the powder is comparable with the reaction half-time $t_{1/2}$, the shapes of the α vs. t kinetic curves are modified, and inflection points are displayed at low α values (i.e. at $\alpha \ll 0.5$). These modifications obliterate the kinetics-type "fingerprints" of these curves, and no meaningful analysis of the data is then possible.

A similar situation may be encountered when the formation of a continuous product layer (cf. Fig. 1) is delayed, i.e. when X_0 in Eq. (2) becomes comparable with the size of the reacting particles (for more details see the discussion section of this article).

(6) The difference between the inflection points induced in the α vs. t kinetic curves by the occurrence of the above-mentioned initiation time dispersions, and inflection points induced by the occurrence of bulk nucleation-and-growth kinetics (Eqs. (13) and (14)) should be noted. In the latter case the inflection points are located at about the half-reaction stage ($\alpha \approx 0.5$; $t \approx t_{1/2}$), and a kinetic analysis of the data is possible.

Finally, it should be emphasized that the term "particle" is not well defined in powder-related fields and is usually associated with the method of measurement of the particular size distribution (e.g. a "particle" can be associated with a crystallite, an aggregate of crystallites or an agglomerate). In our present context the term "particle" refers to the smallest solid entity reacting by the contracting-envelope morphology (Fig. 1) and is not necessarily identical with the powders aggregates as determined by microscopic (e.g. scanning electron microscopy) or sedimentation measurements. An example of such an extreme difference has been demonstrated in the discussion section, for the reaction of polycrystalline bulk samples occurring by fast grain boundary diffusion. In this case the term "particles" is in fact related to grains within the bulk sample. This issue, however, is important only for the determination of absolute values of the intrinsic kinetic parameters (which requires the calculation of averaged size parameters) but is irrelevant to the identification of the type of kinetics and the determination of pressure–temperature trends (which, as stated above, do not require knowledge of particle shapes or size distributions).

Acknowledgements

This work was supported by a grant from the Israel Council for Higher Education and the Israel Atomic Energy Commission.

Appendix A: Nomenclature

a_i	constants appearing in the equation which relates the reacted fraction to the reaction displacement (Eq. (1)); they depend on the shape and size of reacting samples
A	dimension of a symmetric particle (e.g. a sphere or cube)
$\langle A_n \rangle$	nth average moment of A
$D(R)$	size distribution function of the particles composing the powder
$D(T)$	(temperature-dependent) diffusivity of the reacting gas atoms in the product layer
E_a	apparent activation energy
$F_{r,g}(\alpha)$	function of the reacted fraction α, which for a given type of kinetics r (r≡CV or D or NG), and geometrical shape g, yields a linear time dependence (Eq. (3)); in some cases, when one of these subscripts (i.e. either r or g) are specified in the text, this subscript in omitted; usually, for spherical symmetry the subscript g≡s is omitted.
$G1$, $G2$	gaussian size distribution functions (Table 2)
H	thickness of a plate-shaped sample
H_c	height of a cylindrically shaped sample
k	kinetic constant related to the intrinsic kinetic parameters
k_D	diffusion-related kinetic constant (Eq. (7))
k_{NG}	nucleation-and-growth-related kinetic constant
K_g	constant related to the geometrical shape of growing nuclei
$L1$, $L2$	long-normal size distribution functions (Table 2)
M	"marker" parameter used for the Monte Carlo simulation of initiation time distribution
n	integer number
P	working pressure
$P_e(T)$	equilibrium pressure of the product phase (temperature dependent)
R	radius of a spherical particle
R_c	radius of a cylindrically shaped sample
R^e	"spherical-equivalent" radius of a non-spherical particle
R_{min}	radius of the smallest particle composing the powder
$\langle R_n \rangle$	nth average moment of R (Eq. (29)) (in some cases, $\langle R_1 \rangle$ is denoted as $\langle R \rangle$)
t	reaction time
$t_{1/2}$	reaction half-time (for $\alpha = 0.5$)
t_0	time required to attain a continuous product layer, coating the reacting particle (the corresponding initial thickness of product layer X_0)
T	absolute temperature
U	product interface velocity in the reacting matrix (U is either constant or time dependent $U(t)$)
$v_i(t)$	reacted volume (at t) of the ith particle in the powder
$V_r(t)$	total reacted volume (at time t)
V_0	initial volume of the sample
$X(t)$	reaction displacement, at time t (given by Eq. (2))

X_0 initial layer thickness when a continuous product layer first forms on the reacting sample (at $t=t_0$).

$y(T)$ composition limit of the hydride phase (at temperature T)

$Z_0(P, T)$ equilibrium excess hydrogen dissolved in the hydride under the experimental P–T conditions

Greek letters

α reacted fraction

$\alpha_{r,g}(t)$ functional time dependence of the reacted fraction, for a given type of kinetics r (r ≡ CV or D or NG; see respective notations) and geometrical shape g, of a reacting particle (g ≡ s, w etc.); in some cases, one of these subscripts (i.e. either r or g) is omitted (when this subscript is specified in the text)

δ smallest dimension of a given shape (e.g. the thickness of a disc, or the radius of a wire)

$\langle\delta_n\rangle$ nth average moment of δ

ϵ volume ratio of product to reactant

λ_a axial ratio of a given shape ($\lambda_a=1$ for a sphere, $\lambda \ll 1$ for a wire and $\lambda_a \gg 1$ for a plate)

ρ weight density of the material

σ standard deviation of the particle size distribution function

σ_t standard deviation of the initiation time distribution

τ $t/t_{1/2}$, reduced time

τ_m value of τ where an inflection point occurs in the $\alpha_{NG}(\tau)$ curves (Eq. (20))

τ_r maximum range of τ for a given type of kinetics (r ≡ CV, D or NG), i.e. $\alpha_r=1$ at $\tau=\tau_r$

τ_r^* value of τ when $\alpha=0.99$ for a given type of kinetics r

Subscripts

c cylinder
CV constant-velocity kinetics
d disk
D diffusion-controlled kinetics
g geometrical shape
NG nucleation-and-growth kinetics
p plane
s sphere
w wire

References

[1] N. Gérard and S. Ono, in L. Schlapbach (ed.), *Hydrogen in Intermetallic Compounds II,* Springer, Berlin, 1992, Chapter 4, pp. 165–195.

[2] J.L. Stakebake, *J. Alloys Comp., 187* (1992) 271.

[3] O. Boser, *J. Less-Common Met., 46* (1976) 91.

[4] H. Oesterreicher, J. Clinton and H. Bittner, *Mater. Res. Bull., 11* (1976) 1241.

[5] S. Tanaka, J.D. Clewley and T.B. Flanagan, *J. Less-Common Met., 56* (1977) 137.

[6] L. Belkbir, E. Joly, N. Gérard, J.C. Achard and A. Percheron-Guegan, *J. Less-Common Met., 73* (1980) 69.

[7] L. Belkbir, E. Joly and N. Gérard, *J. Less-Common Met., 81* (1981) 199.

[8] C.N. Park and J.Y. Lee, *J. Less-Common Met., 83* (1982) 39.

[9] M. Miyamoto, K. Yamaji and Y. Nakata, *J. Less-Common Met., 89* (1983) 111.

[10] P.D. Goodell and P.S. Rudman, *J. Less-Common Met., 89* (1983) 117.

[11] A.J. Goudy, D.G. Stokes and J.A. Gazzillo, *J. Less-Common Met., 91* (1983) 149.

[12] P. Dantzer and E. Orgaz, *Z. Phys. Chem., NF, 164* (1989) 1267.

[13] P. Dantzer and E. Orgaz, *J. Less-Common Met., 147* (1989) 27.

[14] M.H. Mintz and J. Bloch, *Prog. Solid State Chem., 16* (1985) 163.

[15] J. Bloch and M.H. Mintz, *J. Less-Common Met., 81* (1981) 301.

[16] E. Efrom, Y. Lifshitz, I. Lewkowicz and M.H. Mintz, *J. Less-Common Met., 153* (1989) 23.

[17] Y. Levitin, J. Bloch and M.H. Mintz, *J. Less-Common Met., 175* (1991) 219.

[18] D. Sarussi, I. Jacob, J. Bloch, N. Shamir and M.H. Mintz, *J. Alloys Comp., 191* (1993) 91.

[19] N. Bronfman, J. Bloch, M.H. Mintz, D. Sarussi and I. Jacob, *J. Alloys Comp., 177* (1991) 183.

[20] P.W.M. Jacobs and F.C. Tompkins, Classification and theory of solid reactions, in W.E. Garner (ed.), *Chemistry of the Solid State,* Butterworth, London, 1955, pp. 184–212.

[21] S.F. Hulbert, *Br. Ceram. Soc., 6* (1969) 11.

[22] J.H. Sharp, G.W. Brindley and B.N.N. Achar, *J. Am. Ceram. Soc., 50* (1967) 484.

[23] G.M. Schwab, in J.W. Mitchell, R.C. DeVries, R.W. Roberts and P. Cannon (eds.), *Reactivity of Solids,* Wiley–Interscience, New York, 1969, pp. 163–169.

[24] K.J. Gallagher, in G.M. Schwab (ed.), *Reactivity of Solids,* Elsevier, New York, 1965, pp. 192–203.

[25] P.C. Kapur, *J. Am. Ceram. Soc., 56* (1973) 79.

[26] M. Avrami, *J. Chem. Phys., 7* (1939) 1103; *J. Chem. Phys., 8* (1940) 212.

[27] B.V. Erofeyev, *Ct. R. Akad. Sci. USSR, 52* (1946) 511.

[28] D.A. Young, *Decomposition of Solids,* Pergamon, Oxford, 1969.

[29] R.E. Carter, *J. Chem. Phys., 34* (1961) 2010; *J. Chem. Phys., 35* (1961) 1137.

[30] G. Valensi, *C.R. Acad. Sci., 202* (1936) 309.

[31] M. Abramowitz and I.A. Stegun, *Handbook of Mathematical Functions,* Dover Publication, New York, 1972, p. 885.

[32] J. Bloch, D. Brami, A. Kremner and M.H. Mintz, *J. Less-Common Met., 139* (1988) 371.

[33] W. Zhang, J. Cimato and A.J. Goudy, *J. Alloys Comp., 201* (1993) 175.

[34] J. Bloch, Z. Hadari and M.H. Mintz, *J. Less-Common Met., 102* (1984) 311.

[35] J. Bloch, *J. Alloys Comp.,* in press.

[36] A. Osovitzky, J. Bloch, M.H. Mintz, H. Vazana and I. Jacob, *Int. Symp. M–H Systems, November 1994, Japan.*